Propeller-like Multicomponent Microstructures: Self-Assemblies of Nanoparticles of Poly(vinyl alcohol)-Coated Ag and/or Cu_2O

Wei-Tai Wu, Yusong Wang, Lei Shi, Wenmin Pang, Qingren Zhu,* Guoyong Xu, and Fei Lu

Hefei National Laboratory for Physical Sciences at the Microscale, Structure Research Laboratory, University of Science and Technology of China, Chinese Academy of Sciences, Hefei 230026, China

Received: April 5, 2006; In Final Form: June 6, 2006

Novel propeller-like multicomponent microstructures, which are actually self-assemblies of nanoparticles of poly(vinyl alcohol) (PVA)-coated Ag and/or Cu_2O, were synthesized in aqueous solution of amphiphilic polyvinylacetone (PVKA) (ketalization degree $D_H = 0.549$), via one-step in situ reduction of Ag^+ and Cu^{2+} under γ-ray irradiation, utilizing the low hydrolysis rate of PVKA in the dilute acidic solution. Herein, PVA chains are obtained from hydrolyzed PVKA. The reaction mechanism and the formation mechanism are proposed. The room temperature photoluminescence spectrum has also been applied to explore the optical property.

Introduction

The self-assembly of inorganic, organic, or inorganic−organic hybrid nanoparticles is a theme that runs through chemistry, biology, and material science. The distinct properties of the nanoparticles can be harnessed in assemblies with new collective properties and potential applications in areas such as optics, electronics, and magnetic storage.[1−4] A wide variety of nano-, micro-, or mesoscale self-assemblies, such as AB-, AB_2-, AB_5-, or AB_{13}-type binary superlattices, CuO dandelions, polypyrrole dendrites, and various assemblies of alkane ligand-capped inorganic nanoparticles, have been generated by diverse methods, including electrophoretic deposition, Langmuir−Blodgett technique, magnetic fields, nucleation under bacterial S-layers, and physical confinement, etc., based on different driving mechanisms.[1−10] Generally, self-assembly occurs mainly through non-covalent interactions such as van der Waals, hydrogen bonding, hydrophilic/hydrophobic, electrostatic, donor and acceptor, and metal-ligand coordination networks.[11] Nevertheless, the self-assembly of nanoparticles into superstructures, particularly three-dimensional (3D) superstructures, poses a formidable challenge, and knowing how to utilize different routes in an orthogonal fashion to obtain novel 3D superstructures is still one of the key requirements for future development in this area.

Presently, polyvinylacetone (PVKA) is known to be a hydrolyzable polymer, its hydrolysis time being controlled by both ketalization degree D_H and pH of water.[12] The lower the initial ketalization degree, the easier the deketalization proceeds in acidic water; and the closer the pH value to neutral, the lower the hydrolysis rate. In particular, the hydrolysis rate of PVKA ($D_H > 0.3$) in water having a pH value that is kept close to neutral is very low; for example, it takes >24 days to complete hydrolysis of amphiphilic PVKA ($D_H \approx 0.5$). Our interests stem from the properties of PVKA. Among the investigations, one focus is the preparation of desirable micro-/nanomaterial.[13−15] For example, we recently reported that dendritic multicomponent assemblies of poly(vinyl alcohol) (PVA) colloidal particles with embedded Ag and/or Cu_2O nanocrystals could be control-synthesized in aqueous solution of amphiphilic PVKA using $AgNO_3$ and $Cu(NO_3)_2$ as the metal sources, utilizing the properties of PVKA.[15] These results indicate the probability of the research of PVKA on structural construction and utilization. Establishing an effective method to prepare desirable micro-/nanostructures is an increasing interest in chemistry and nanotechnology and also a challenge in PVKA study.

Modifying the composition of the source materials can drastically change the morphology of the grown micro-/nanostructure, which provides an efficient strategy to synthesize novel micro-/nanostructures.[16] In this paper, our work is focused on the synthesis of novel propeller-like multicomponent microstructures, which are actually self-assemblies of nanoparticles of PVA-coated Ag and/or Cu_2O, via one-step in situ reduction of Ag^+ (from $AgNO_3$) and Cu^{2+} (from $CuSO_4$) in aqueous solution of amphiphilic PVKA ($D_H = 0.549$) under γ-ray irradiation. Noble metal Ag and the p-type semiconductor Cu_2O have been the subject of much intensive research today due to their unique properties and their potential applications as promising materials in the fields of solar energy conversion, micro-/nanoelectronics, catalysis, and biosensors.[17−23] The incorporation of the Ag and/or Cu_2O nanoparticles into PVA matrixes could exhibit novel properties because the nanoparticles are strongly affected by the surrounding matrix as well as because the particles are closely spaced in the matrixes, which therefore will extend their utility in the as-obtained material; moreover, the unique properties of assemblies of nanoparticles, for example, inter-nanoparticle electronic, photonic, and energy transfer, would also make them essential not only to the production of novel devices but also to the understanding of fundamental phenomena at the nanoscale and even to the understanding of some processes in living organisms.[3,24,25]

Experimental Section

Synthesis Method. PVKA ($D_H = 0.549$) was synthesized by ketalizing PVA (degree of polymeration = 1750 ± 50, saponification value > 99%) with acetone and with PTS/TBAB (*p*-toluenesulfonic acid and tetrabutylammonium bromide) as catalyst, as outlined in a previous publication.[12]

$AgNO_3$ (4.7×10^{-3} mol) and $CuSO_4 \cdot 5H_2O$ (1.6×10^{-3} mol) were added into 20 mL of PVKA (30 g L^{-1}) aqueous solution

* Corresponding author (fax +86-551-3602803; e-mail zhuqr@ustc.edu.cn).

10.1021/jp062121c CCC: $33.50
Published on Web 07/11/2006

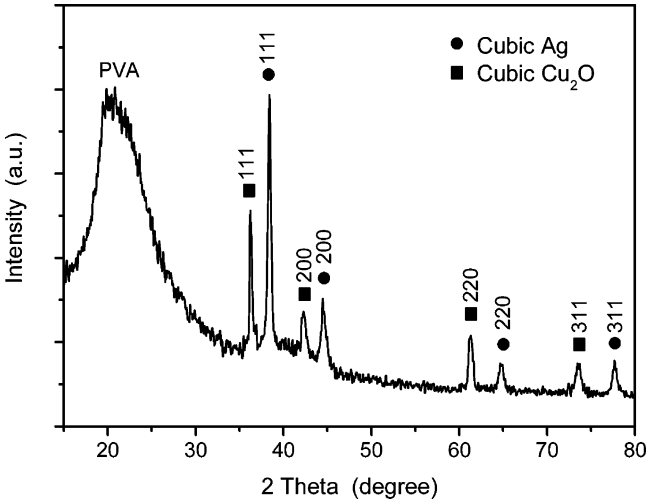

Figure 1. XRD patterns of the propeller-like microstructures obtained after irradiation for 2.0×10^5 Gy at a dose rate of 34 Gy min^{-1}.

with vigorous stirring for 30 min to yield a uniform white floccule, which was then aerated with N_2 for 30 min to remove the oxygen solvated in the system and then irradiated with a 2.5×10^{15} Bq ^{60}Co γ-ray source at a dose rate of 34 Gy min^{-1} for an absorbed dose of 2.0×10^5 Gy. The whole reaction was performed under ambient conditions. The resulting gray floccule was washed with distilled water and ethanol repeatedly to remove ions and possible remnants in the final product.

Characterization. The samples were identified by X-ray powder diffraction pattern (XRD), recorded on a MAC Science Co. Ltd. MXP 18 AHF X-ray diffractometer with monochromatized Cu Kα radiation ($\lambda = 1.54056$ Å). X-ray photoelectron spectra (XPS) were obtained with a VG Smart IQ$^+$ Thermo Electron Co. ESCALAB 250 XPS spectrometer. TEM and HRTEM images were obtained on a Hitachi H-800 transmission electron microscope at an accelerating voltage of 200 kV and on a JEOL-2010 high-resolution transmission electron microscope, also at 200 kV, respectively. SEM images were obtained on an FEI Sirion 200 field emission scanning electron microanalyzer using conventional sample preparation and imaging techniques. The pH values were obtained on a Shanghai Precision & Scientific Instrument Co. Ltd. pHS-25 pH-meter. FTIR spectra were recorded with a Nicolet Instrument Co. MAGNA-IR 750 FTIR spectrometer. The room temperature photoluminescence (PL) spectra were obtained on a Jobin Yvon Co. FLUOROLOG-3-TAU Steady-state/Lifetime spectrofluorometer.

Results and Discussion

XRD Patterns. XRD was used to examine the crystal structure of the sample. Figure 1 shows a typical XRD pattern of the propeller-like structures obtained after irradiation for 2.0×10^5 Gy at a dose rate of 34 Gy min^{-1}. Those diffraction peaks can be indexed to the (111), (200), (220), and (311) planes of the *fcc* structure of Ag (JCPDS No. 04-0783), the (111), (200), (220), and (311) planes of the cubic structure of Cu_2O (JCPDS No. 05-0667), and those strong crystalline reflections (identified as the superposition of $10\bar{1}$ and 101 reflections) due to the microcrystalline domains of PVA.[26] No impurity peaks from CuO, or new composites of Ag/Cu_2O (the signals maybe too weak), were found in the experimental range.

XPS Measurements. Further evidence for the purity and composition of the product was obtained by XPS measurements. The XPS analysis (Figure 2) shows that the sample contains

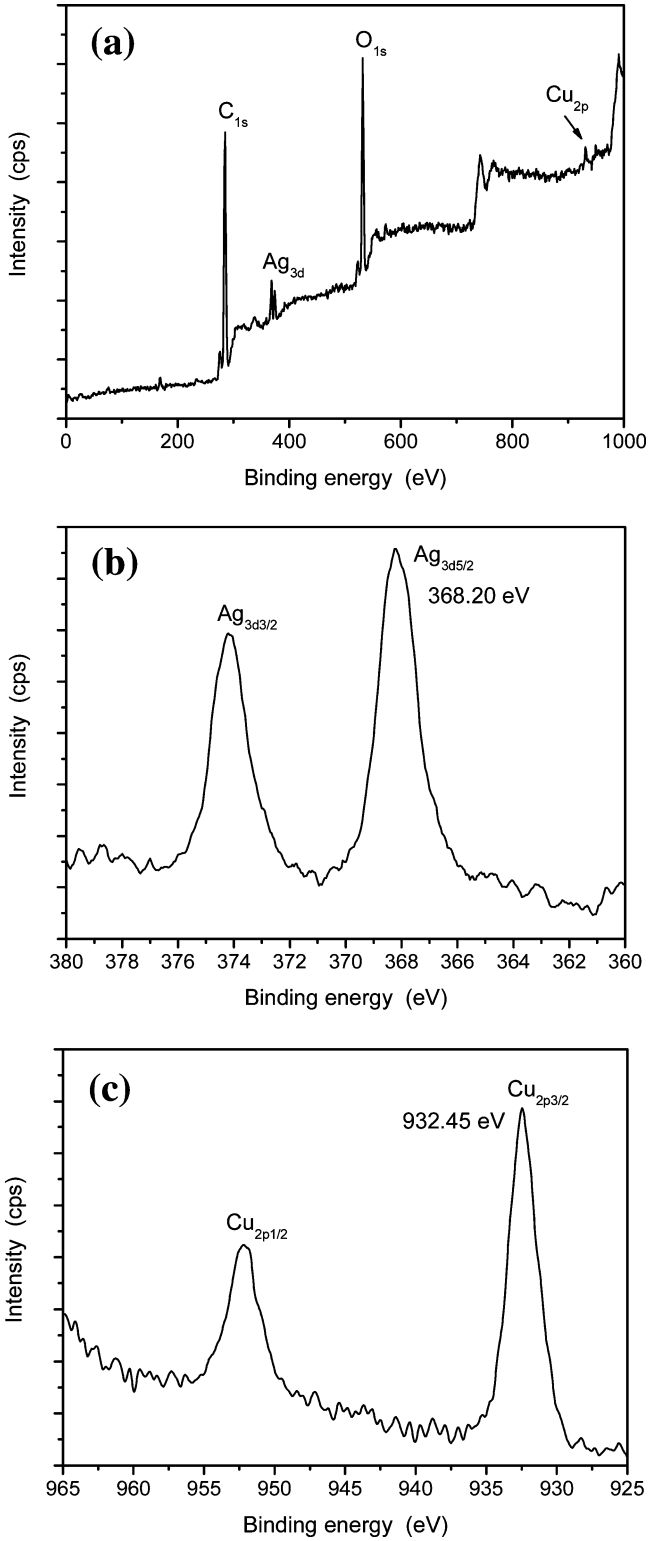

Figure 2. (a) XPS survey spectrum of the propeller-like microstructures obtained after irradiation for 2.0×10^5 Gy at a dose rate of 34 Gy min^{-1}; higher resolution spectra of (b) Ag 3d region and (c) Cu 2p region.

Ag (1.30%, molar content), Cu (1.28%), O (27.40%), and C (70.03%). Higher resolution spectra were also recorded in the Ag 3d and Cu 2p regions. Figure 2b shows the XPS spectrum in the Ag 3d5/2 and Ag 3d3/2 binding energy region with a spin−orbit separation of 6.00 eV. The Ag 3d5/2 peak is centered at 368.20 eV (kinetic energy is ≈503.4 eV), which is close to that of pure metallic Ag. Figure 2c shows the XPS spectrum in

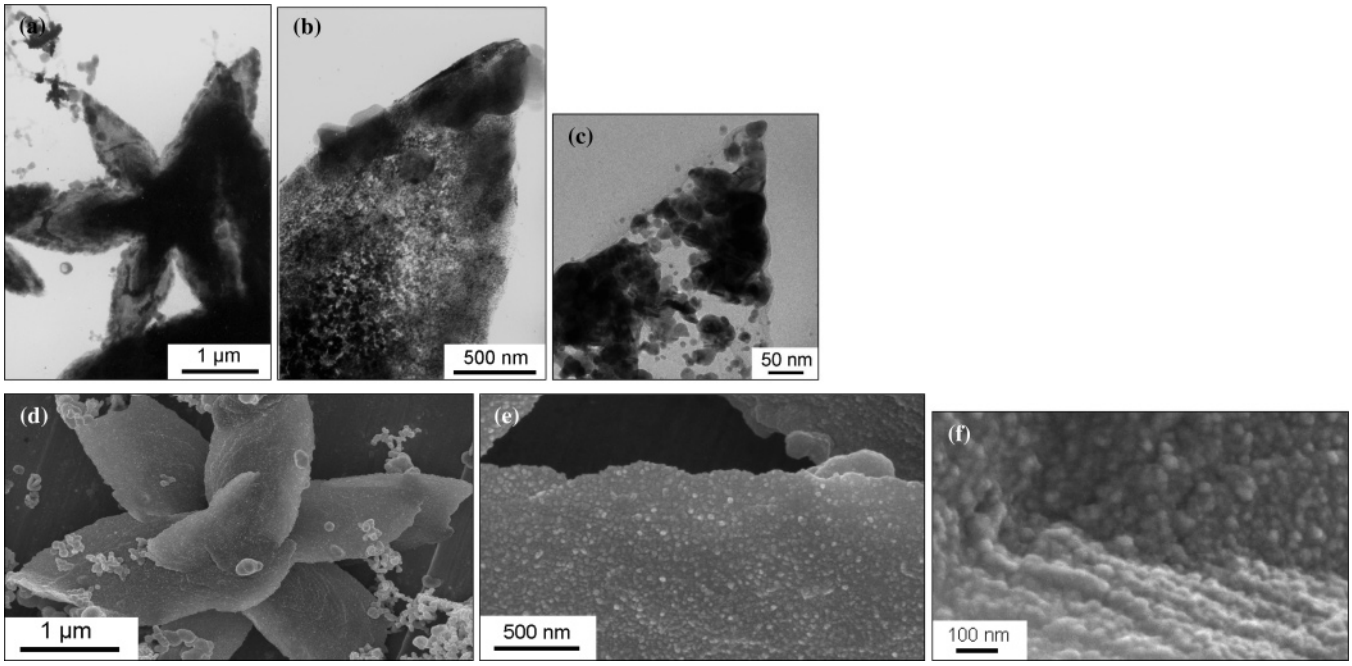

Figure 3. (a) Typical TEM image of the propeller-like microstructures obtained after irradiation for 2.0×10^5 Gy at a dose rate of 34 Gy min^{-1}; (b, c) enlarged TEM images; (d) corresponding SEM image; (e, f) enlarged SEM images.

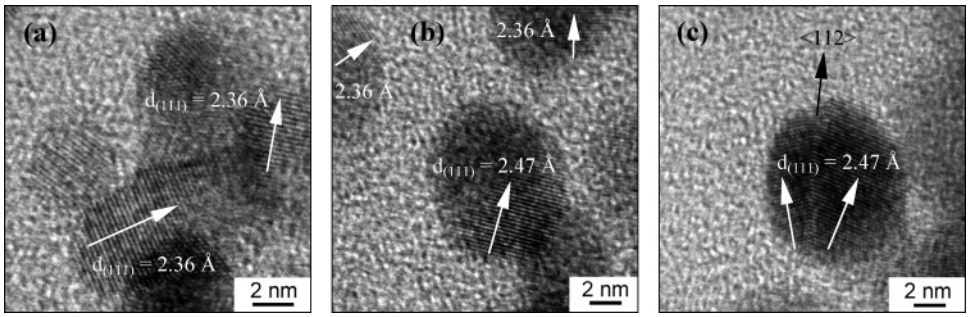

Figure 4. Typical lattice-resolved HRTEM images of the propeller-like microstructures obtained after irradiation for 2.0×10^5 Gy at a dose rate of 34 Gy min^{-1}, showing (a, b) the single crystal with high crystallinity and (c) a twin structure in a single Cu_2O nanocrystal with the twinning orientation ⟨112⟩.

the Cu 2p3/2 and Cu 2p1/2 binding energy region with a spin−orbit separation of 19.75 eV. The Cu 2p3/2 peak is centered at 932.45 eV (kinetic energy is ≈916.5 eV), which is close to that of Cu_2O, and no peaks due to CuO (≈933.6 eV) were observed.[20]

Electron Microscope Images. Figure 3a presents a typical TEM image of the obtained propeller-like microstructures. Enlarged TEM images (Figure 3b,c) show that the propeller-like microstructure is not a metallic (or polymeric) statue as a whole, but a supramolecular structure of assembled smaller colloidal particles of PVA-coated Ag and/or Cu_2O. The elegant propeller-like microstructures represent a very wide variety of growth, in which one colloidal particle after another is formed and then diffuses, sticking to the growing structure. Generally, during the assembling process, the self-assemblies are known to be formed by long-range attractive interaction[27,28] and lateral capillary force (LCF)[29,30] of the colloidal particles. The characteristic of this morphology is also reflected in the SEM images (Figure 3d−f). Furthermore, as shown in Figure 3d, the propeller-like microstructures remain in their sixfold arrays of nonparallel nanovanes, the surfaces of which are rough with steps, around the central axes (may be also described as a helical growth). Cursorily, the percent yield of the propeller-like microstructures is ≈60% as estimated from the electron microscope images of the examined samples.

Moreover, the crystalline nature of Ag and/or Cu_2O embedded in the PVA particles was confirmed by lattice-resolved HRTEM images (Figure 4a,b). The lattice spacing of 2.36 Å is clearly observed corresponding to that of the (111) plane for the Ag phase and the spacing of 2.47 Å corresponding to that of the (111) plane for the Cu_2O phase. Most Cu_2O nanocrystals (≈90%) are single crystal; however, twin structures of a single Cu_2O nanocrystal were also observed (Figure 4c, occurring in this same form in ≈10% of all Cu_2O nanocrystals). Twinning is one of the most popular planar defects in *fcc* structures.[31] Twinning is the result of two subgrains sharing a common crystallographic plane; thus, the structure of one subgrain is the mirror reflection of the other by the twin plane. The twin plane is (111), and the twinning orientation is ⟨112⟩ (Figure 4c). Generally, twinning can be a result of deformation and/or dislocation motions in a cubic system. In our case, we believe twinning is sometimes induced due to the volume change of the two phases when Cu^{2+} transforms to Cu_2O.[17] However, no twin structure of Ag nanocrystals was observed in our experiment.

Some Insight into the Reaction Mechanism. The pH value dropped dramatically from 6.3 for the starting initial solution to 3.8 for the residual solution after irradiation for 2.0×10^5 Gy at a dose rate of 34 Gy min^{-1}, implying that the solution

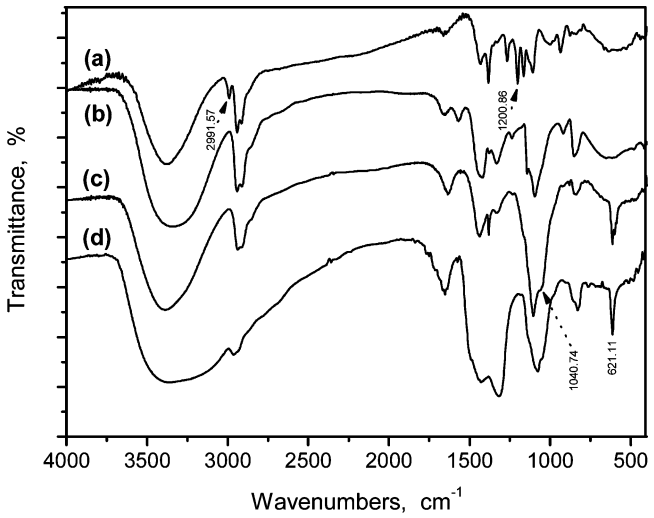

Figure 5. FTIR spectra: (a) pure PVKA; (b) pure PVA; (c) obtained propeller-like microstructures; (d) residual solution after irradiation for 2.0×10^5 Gy at a dose rate of 34 Gy min^{-1}.

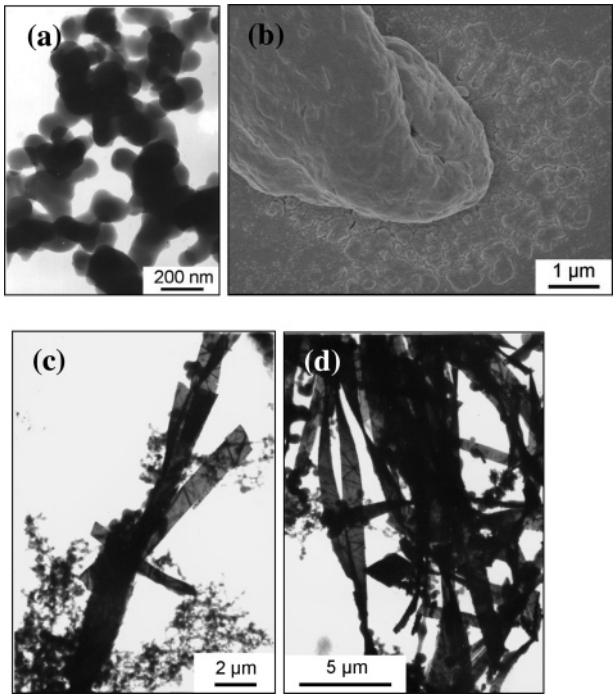

Figure 6. TEM/SEM images of the product obtained after irradiation for an absorbed dosage of 1.8×10^5 Gy at different dose rates: (a) 105 Gy min^{-1} and (b) corresponding SEM image; (c) 92 Gy min^{-1}; (d) 82 Gy min^{-1}, showing the effect of the dose rate on the morphology. Under a much higher dose rate (>105 Gy min^{-1}), most obtained products were massive gels.

becomes more acidic, which would lead to the slow hydrolysis of PVKA.[12−15]

The FTIR spectrum (Figure 5) of the obtained propeller-like microstructures is almost the same as that of pure PVA, which shows several absorption peaks corresponding to ν_{C-O} (1094.6 cm^{-1}), ν_{C-C} (916.0 cm^{-1}), and γ_{CH2} (851.1 cm^{-1}) of the alcohol unit, whereas those peaks corresponding to the ν_{C-O-C} (1200.9 cm^{-1}) and ν_{CH2} (2991.6 cm^{-1}) in the ketal-ring unit, which are similar to the ones appearing for pure PVKA, gradually become lower and cannot be observed finally (>4.0×10^4 Gy). Those results indicate that the PVKA was hydrolyzed in the acidic solution during the reaction and that the slow hydrolysis process of PVKA leads to slow cross-linking of PVA, which favors the formation of the propeller-like microstructures (see below). Furthermore, the absorption peak located at 1040.7 cm^{-1} (assigned to the ν_{C-O-C}) indicates the cross-linked PVA, and this relatively weak sign indicates the low cross-link density of PVA; this result coincides with that shown by XRD patterns, as revealed by the strong crystalline reflections due to the microcrystalline domains of PVA;[26] that is, the material still contains a rather high number of alcohol units. In addition, it is very significant that the complete hydrolysis time (≈1.5 days) is greatly shortened compared with a previous result (>10 days).[12]

In Figure 5, the FTIR peak of Cu_2O nanocrystals shows a main peak at ≈621.1 cm^{-1}, which slightly shifts toward blue compared with that of bulk Cu_2O (≈613 and ≈146 cm^{-1}).[22] The slight shift in peak position could be the effect of reduction in particle size. Due to the limitation of the spectrometer, the low-frequency mode could not be observed. No infrared active mode corresponding to CuO (≈500 cm^{-1}) could be seen.

On the basis of the above analysis and previous results,[13−15,19,21,32,33] the reaction that occurred under γ-ray irradiation may be explained as follows:

$$H_2O \xrightarrow{\text{irradiation}} e_{aq}^-, H_3O^+, H^\bullet, H_2, {}^\bullet OH, H_2O_2$$

$$PVKA + Ag^+ + H_2O \rightarrow PVA + Ag + H^+ + \text{acetone}$$

$$PVA(H) + {}^\bullet OH \rightarrow PVA^\bullet + H_2O$$

$$Ag^+ + e_{aq}^-/PVA^\bullet \rightarrow Ag$$

$$Cu^{2+} + e_{aq}^-/PVA^\bullet \rightarrow Cu^+$$

$$Cu^+ + H_2O \rightarrow Cu(OH) + H^+$$

$$2Cu(OH) \rightarrow Cu_2O + H_2O$$

$$2PVA^\bullet \rightarrow PVA-PVA \text{ (cross-linked polymer)}$$

Many products initially generated from the radiolysis of aqueous solution by γ-ray irradiation are well understood. Some of them have reducing potential, whereas others have oxidizing ability. The irradiation cross-linking of PVA molecules is known to be induced mainly by hydroxyl radicals $^\bullet OH$ in aqueous solution, resulting in a 3D network of the hydrogel. Ag^+ ions are known to have very high reactivity with both e_{aq}^- and $^\bullet OH$. However, under the present experimental conditions, $^\bullet OH$ almost exclusively reacts with PVA, and the reduction of Ag^+ ions takes place by strongly reducing both e_{aq}^- and the polymeric radicals $PVA^\bullet$ (having a structure similar to that of alcohol radicals) formed by H atom abstraction reaction from PVA chains by $^\bullet OH$.[33] It should be mainly e_{aq}^-, maybe as well as $PVA^\bullet$, that reduces the Cu^{2+} ions to Cu^+ ions, which are unstable in aqueous solution and form unsolvable Cu(OH) under the present conditions (pH 6.3−3.8), and translates into Cu_2O finally.[19,21]

Effect of the Dose Rate and the Absorbed Dosage on the Morphology. Under higher dose rates (>82 Gy min^{-1}, Figure 6), other structures were obtained, such as nanoribbons and irregular nanoparticles (most of them aggregate together). Under much higher dose rates (>105 Gy min^{-1}), most obtained products were massive gels. Assisted by the electron diffraction patterns (ED), most of the nanoparticles shown in Figure 6a were polymer particles with amorphous nature, and a few of these nanoparticles were embedded with very tiny metal/oxide clusters; these coexist with the massive gels (Figure 6b). The

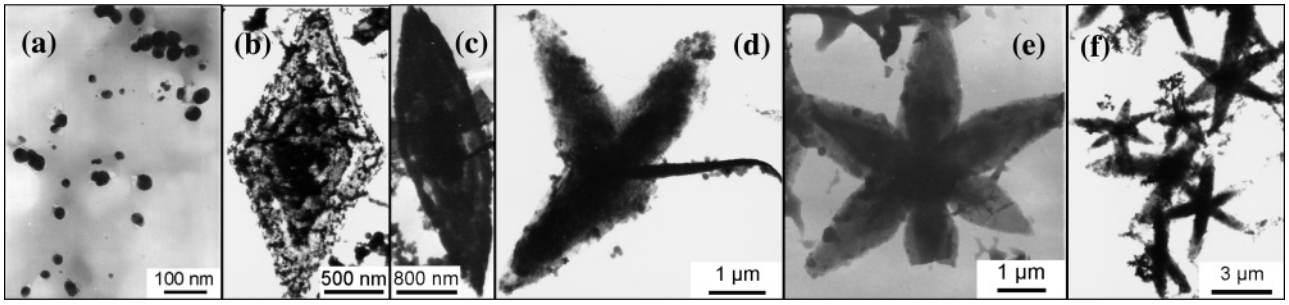

Figure 7. TEM images of the product obtained after irradiation at a dose rate of 34 Gy min^{-1} for various absorbed dosages: (a) 8.0×10^3 Gy; (b) 4.0×10^4 Gy; (c) 6.2×10^4 Gy; (d) 1.1×10^5 Gy; (e) 1.5×10^5 Gy; (f) 1.8×10^5 Gy.

dominant structure shown in Figure 6c,d was metal/oxide nanoribbons, which coexist with the nanoparticles described above. Under such a high dose rate, the uncontrollable cross-linking of polymer to massive gels or polymer particles becomes faster, which is much easier than the reduction of metal ions, leading to the confined growth of the (few) embedded Ag/Cu_2O nucleus in the gel matrix; simultaneously, the rapid nucleation and growth of the Ag/Cu_2O excluded in the gel matrix leads to a different architecture without polymer phase. This suggests that the slow irradiation reduction process may favor the formation of the present propeller-like microstructures (34 Gy min^{-1}, Figure 7), and the formation of polymer-coated Ag/Cu_2O nanoparticles takes place during Ag/Cu_2O incorporation into the polymer core; then the oriented aggregation of these polymer-coated Ag/Cu_2O nanoparticles leads to the propeller-like microstructures finally. Note that the very low dose rate may also favor the formation of propeller-like microstructures, but it would take a much longer time. Moreover, the presence of a moderate amount of propan-2-ol usually could slow the reaction, because propan-2-ol could scavenge $^{\bullet}OH$ and $H^{\bullet}$;[32,33] however, in our experiments, it is incomprehensible that the presence of even a small amount of propan-2-ol always results in only disordered nanoparticles (Figure S1, Supporting Information).

The effect of the absorbed dosage was also studied, and results reveal that the formation of the propeller-like microstructures needs a moderate absorbed dosage (Figure 7). Perfect propeller-like microstructures with sixfold arrays of nonparallel nanovanes could not be obtained when irradiated for a minor dosage (34 Gy min^{-1}, $< 1.8 \times 10^5$ Gy). When the propeller-like microstructures have formed, prolonging the reaction time could lengthen the central axes to a certain extent; that is, when irradiated for a moderately larger dosage, the number of nanovanes would increase (but still form sixfold arrays on top view). However, with a much larger dosage, the central axes could not be further lengthened; contrarily, a much larger dosage does not favor the formation process, perhaps due to the higher cross-link density. When irradiated for a much larger dosage ($>4.5 \times 10^5$ Gy) at a dose rate of 34 Gy min^{-1}, the present propeller-like microstructures tended to aggregate with each other and the propeller-like structures were destroyed, resulting in irregular shapes finally.

Moreover, control experiments also showed that the propeller-like microstructures were not obtained in any cases when PVA was substituted for PVKA. PVA has many reactive short side chains (hydroxyl groups), which makes the cross-linking of PVA very easy through the cross-linkage among hydroxyl groups and the carbons on the main-chain backbones;[32,34,35] the rapid cross-linking reaction rate, as well as the high cross-link density, goes against the oriented aggregation of the polymer-coated Ag/Cu_2O nanoparticles to the propeller-like microstructures.

These studies also lead us to conclude that PVKA clearly plays a key role in our experiments. The backbone of an incompletely hydrolyzed PVKA chain contains the rigid six-membered ketal rings; the existence of these rigid rings would make the neighboring groups become unreactive, because of the spatial interactions.[14,15] In the present study, it is possible that the slow hydrolysis process of PVKA leads to slow cross-linking of the polymer, resulting in low cross-link density of the polymer during the growth process of the propeller-like microstructures, which favors the formation of the propeller-like microstructures; furthermore, as it still contains a rather high number of alcohol units, the polymer may also be a kind of capping material, which usually acts as steric stabilizer.

Some Insight into the Formation Mechanism. Some insight into the formation mechanism has also been obtained by examining TEM images (Figure 7) of the products obtained at earlier stages (that is, irradiated for a lower dosage at a dose rate of 34 Gy min^{-1}).

An examination of the samples obtained after irradiation for a smaller dosage ($\leq 8.0 \times 10^3$ Gy) revealed polymer spherical nanoparticles (30−60 nm) with smaller Ag/Cu_2O clusters embedded in the polymer gel matrix (Figure 7a). Obviously, reduction of Ag^+ and Cu^{2+} ions and formation of an interlinked gel structure occurred simultaneously. After irradiation for 4.0×10^4 Gy (Figure 7b), the TEM image shows that these small colloidal particles with embedded Ag/Cu_2O clusters aggregated in an oriented manner to form rhombic supramolecular structures, which clearly have many steps around the central axes (coaxial rhombus, coupled with the SEM image shown in Figure S2a, Supporting Information). The interaction and stabilization of these colloidal particles are not unusual, as the polymer still has many hydroxyl groups and is known as a colloidal stabilizer.[13−15] After irradiation for 6.2×10^4 Gy (Figure 7c), the steps on the surface became somewhat illegible under TEM, because of the incrassation of the coaxial rhombus to form a shuttle-like structure; moreover, it is worth noting that two convex areas appeared on the center (Figures 3d and S2b). Then, these convex areas further developed into two new nanovanes; simultaneously, the foregoing shuttle-like structure evolved into two nanovanes, making these four nanovanes seem to be a helical growth (Figures 7d and S2b). The further growth of these structures leads to the formation of the propeller-like microstructures finally (Figures 3 and 7e,f), which actually involves the adhesion of a particle to a selected seed on contact and allows the particle to diffuse and stick to the growing structure. The formation of the coalesced colloidal particles is considered to originate mainly from long-range attractive interactions.[27,28] Moreover, strong capillary forces would arise owing to the meniscus formed between two particles, and their lateral projection could also drag the particles together, depending

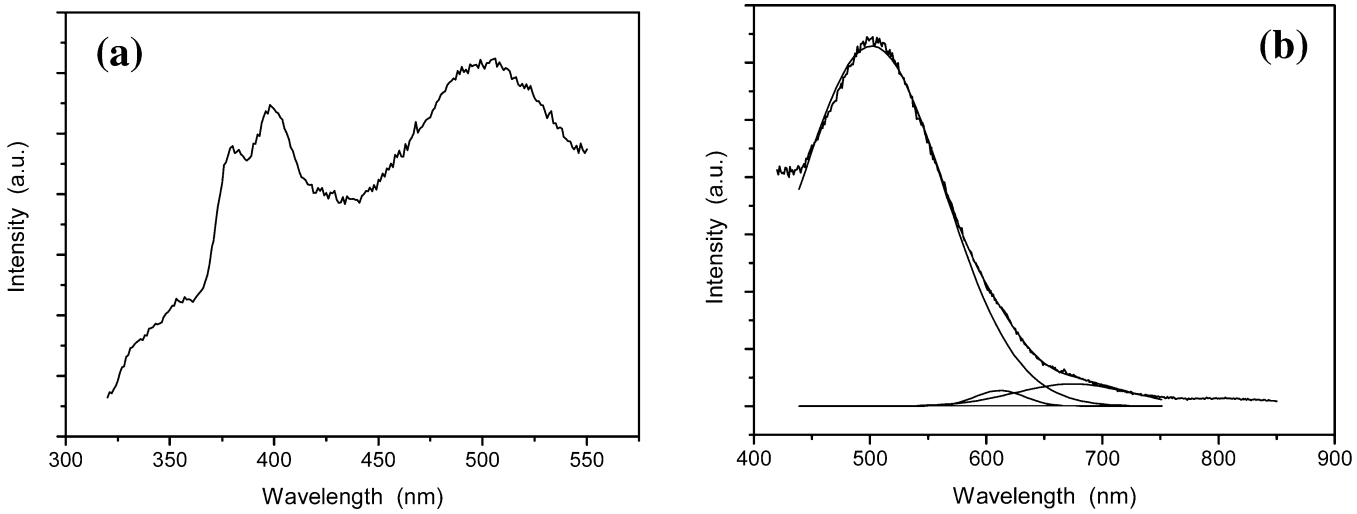

Figure 8. Room temperature PL spectrum of the product obtained after irradiation for 2.0×10^5 Gy at a dose rate of 34 Gy min^{-1}. The excitation wavelength is 290 nm.

inversely on the particle distance; thus, LCF may become another dominant attractive interaction.[29,30]

Optical Properties. The room temperature PL spectrum of the product obtained after irradiation for 2.0×10^5 Gy at a dose rate of 34 Gy min^{-1} was also studied, as shown in Figure 8. The PL spectrum in the 325−850 nm region is composed of two major components. At room temperature, one broad peak (in the range of 450−750 nm) in the visible region and several peaks (in the range of 325−425 nm) in the near-ultraviolet region were observed. Although further theoretical studies may be still required to exactly explain those PL signals and there may be other possibilities, a possible explanation is proposed below.

Theoretical work demonstrated that the PL of noble metals could be viewed as an excitation of electrons from occupied d bands into states above the Fermi level; subsequent electron−phonon and hole−phonon scattering processes lead to energy loss and finally photoluminescent recombination of an electron from an occupied sp band with the hole.[36] PL of Ag clusters has been previously observed at 400 nm, similar to the observed surface plasmon average energy for 13 nm Ag nanoclusters.[37] Furthermore, it is commonly assumed that there is no PL for large metal particles, in which rapid radiationless processes compete effectively with radiative processes.[38] Thus, in the present case, the PL bands (in the range of 325−425 nm, Figure 8a) in the near-ultraviolet region were attributed to the smaller Ag nanoparticles (embedded in polymer). The origin of these strong PL signals is due to the efficient coupling of incident radiation to the surface plasmon of the smaller particles. With the growth of the smaller nanoclusters, the nature of the surface could change the efficiency of the coupling of the excitation radiation to the surface plasmon, and this efficiency is low for the larger particles because of unique surface structures present on the smaller particles; therefore, several peaks in the present PL spectrum may be due to the nonuniform size of the Ag nanoparticles and maybe also depend on the embedding medium.[18,39]

The broad PL band (in the range of 450−750 nm) in the visible region shows some asymmetric, which could be fit with three symmetric peaks (centered at ≈501, ≈612, and ≈675 nm, respectively; Figure 8b). Among them, the peak at ≈501 nm was due to the emission of the smaller Ag nanoparticles, which also comes from the recombination mentioned above.[18,40]

It is known that the energy minimum of the conduction band and the energy maximum of the valance band in Cu_2O are nondegenerate and located at the zone center. Because both of the bands have even parity, electric dipole transitions between the two states are forbidden. An exciton formed from these two bands has to annihilate through other means, thus, as electric quadrupole transitions or via phonon-assisted transitions.[41] The crystal structure of Cu_2O includes two molecules per unit cell, and group theoretical analysis suggests that the phonons have symmetries Γ_{25}^-, Γ_{15}^-, Γ_{12}^-, and Γ_2^- at the Γ point. At room temperature, only one broad near band luminescence is observed. The PL peak at ≈612 nm (2.03 eV, Figure 8b) was attributed to the exciton emission of Cu_2O, which shifts toward the blue (compared to the bulk Cu_2O) caused by the quantum confinement of exciton photogenerated inside the nanoparticle. The PL peak at ≈675 nm (1.84 eV, Figure 8b) may be assigned to the emission of different defect centers and may be attributed to V_O.[23,41]

Conclusions

In summary, we have successfully achieved the controlled synthesis of the propeller-like microstructures, which are actually self-assemblies of PVA colloidal particles with embedded Ag and/or Cu_2O nanocrystals, via one-step in situ reduction of Ag^+ and Cu^{2+} in aqueous solution of amphiphilic PVKA (D_H = 0.549) under γ-ray irradiation, utilizing the low hydrolysis rate of the PVKA in dilute acidic solution. The room temperature PL spectrum has also been applied to explore the optical property, and the PL emissions (for Ag and Cu_2O, respectively) were observed to shift toward the blue due to the quantum confinement effect of the embedded Ag/Cu_2O particles. The present propeller-like multicomponent assemblies could become alternative products to some extent; moreover, the unique properties of assemblies of nanoparticles, for example, inter-nanoparticle electronic, photonic, and energy transfer, would make them essential not only to the production of novel devices but also to the understanding of fundamental phenomena at the nanometer scale and even to the understanding of some processes in living organisms.[3,24,25]

Acknowledgment. This work was supported by the Open Foundation of Structural Research Laboratory of USTC and the Innovation Foundation of USTC for the Postgraduate. We gratefully acknowledge Prof. Shuyuan Zhang for helpful discussion about the HRTEM results.

Supporting Information Available: SEM images (Figure S1) showing disordered nanoparticles obtained in the presence

of propan-2-ol and those (Figure S2) showing steps and the two convex areas. This material is available free of charge via the Internet at http://pubs.acs.org.

References and Notes

(1) Murray, C. B.; Kagan, C. R.; Bawendi, M. G. *Annu. Rev. Mater. Sci.* **2000**, *30*, 545.
(2) Shenhar, R.; Norsten, T. B.; Rotello, V. M. *Adv. Mater.* **2005**, *17*, 657.
(3) Tang, Z.; Kotov, N. A. *Adv. Mater.* **2005**, *17*, 951.
(4) Cölfen, H.; Mann, S. *Angew. Chem., Int. Ed.* **2003**, *42*, 2350.
(5) Redl, F. X.; Cho, K.-S.; Murray, C. B.; O'Brien, S. *Nature* **2003**, *423*, 968.
(6) Shevchenko, E. V.; Talapin, D. V.; Kotov, N. A.; O'Brien, S.; Murray, C. B. *Nature* **2006**, *439*, 55.
(7) Liu, B.; Zeng, H. C. *J. Am. Chem. Soc.* **2004**, *126*, 8124.
(8) Jang, J.; Joon, H. O. *Langmuir* **2004**, *20*, 8419.
(9) Park, S.; Lim, J.-H.; Chung, S.-W.; Mirkin, C. A. *Science* **2004**, *303*, 348.
(10) Hu, J.-S.; Guo, Y.-G.; Liang, H.-P.; Wan, L.-J.; Jiang, L. *J. Am. Chem. Soc.* **2005**, *127*, 17090.
(11) Whitesides, G. M.; Grzybowski, B. *Science* **2002**, *295*, 2418.
(12) Wu, W.-T.; Pang, W.; Wang, Y.; Zhu, Q.; Lu, F.; Xu, G. *Polymer* **2005**, *46*, 3132.
(13) Wu, W.-T.; Pang, W.; Xu, G.; Shi, L.; Zhu, Q.; Wang, Y.; Lu, F. *Nanotechnology* **2005**, *16*, 2048.
(14) Wu, W.-T.; Wang, Y.; Shi, L.; Zhu, Q.; Pang, W.; Xu, G.; Lu, F. *Nanotechnology* **2005**, *16*, 3017.
(15) Wu, W.-T.; Shi, L.; Zhu, Q.; Wang, Y.; Pang, W.; Xu, G.; Lu, F. *Nanotechnology* **2006**, *17*, 1948.
(16) Wang, Z. L. *Mater. Today* **2004**, *7*, 26.
(17) Yin, M.; Wu, C.-K.; Lou, Y.; Burda, C.; Koberstein, J. T.; Zhu, Y.; O'Brien, S. *J. Am. Chem. Soc.* **2005**, *127*, 9506.
(18) Evanoff, D. D.; Chumanov, G. *ChemPhysChem* **2005**, *6*, 1221.
(19) He, P.; Shen, X.; Gao, H. *J. Colloid Interface Sci.* **2005**, *284*, 510.
(20) Deroubaix, G.; Marcus, P. *Surf. Interface Anal.* **1992**, *18*, 39.
(21) Zhu, Y. J.; Qian, Y.; Zhang, M.; Chen, Z.; Xu, D. *Mater. Res. Bull.* **1994**, *29*, 377.
(22) Borgohain, K.; Murase, N.; Mahamuni, S. *J. Appl. Phys.* **2002**, *92*, 1292.
(23) Liu, Y.; Liu, Y.; Mu, R.; Yang, H.; Shao, C.; Zhang, J.; Lu, Y.; Shen, D.; Fan, X. *Semicond. Sci. Technol.* **2005**, *20*, 44.
(24) Maier, S. A.; Kik, P. G.; Atwater, H. A.; Meltzer, S.; Harel, E.; Koel, B. E.; Requicha, A. A. G. *Nat. Mater.* **2003**, *2*, 229.
(25) Alivisatos, P. *Nat. Biotechnol.* **2004**, *22*, 47.
(26) Ricciardi, R.; Auriemma, F.; Rosa, C. D.; Lauprêtre, F. *Macromolecules* **2004**, *37*, 1921.
(27) Wickman, H. H.; Korley, J. N. *Nature* **1998**, *393*, 445.
(28) Horvolgyi, Z.; Mate, M.; Zrinyi, M. *Colloids Surf. A* **1994**, *84*, 207.
(29) Denkov, N. D.; Velev, O. D.; Kralchevsky, P. A.; Ivanov, I. B.; Yoshimura, H.; Nagayama, K. *Nature* **1993**, *361*, 26.
(30) Xia, Y.; Gates, B.; Yin, Y.; Lu, Y. *Adv. Mater.* **2000**, *12*, 693.
(31) Wang, Z. L. *J. Phys. Chem. B* **2000**, *104*, 1153.
(32) Ulanski, P.; Bothe, E.; Rosiak, J. M.; Sonntag, C. V. *Macromol. Chem. Phys.* **1994**, *195*, 1443.
(33) Kumar, M.; Varshney, L.; Francis, S. *Radiat. Phys. Chem.* **2005**, *73*, 21.
(34) Gaddy, G. A.; McLain, J. L.; Steigerwalt, E. S.; Broughton, R.; Slaten, B. L.; Mills, G. *J. Cluster. Sci.* **2001**, *12* (3), 457.
(35) Temgire, M. K.; Joshi, S. S. *Radiat. Phys. Chem.* **2004**, *71*, 1039.
(36) Apell, P.; Monreal, R.; Lundqvist, S. *Phys. Scr.* **1988**, *38*, 174.
(37) Kokkinakis, Th.; Alexopoulos, K. *Phys. Rev. Lett.* **1972**, *28*, 1632.
(38) Félix, C.; Sieber, C.; Harbich, W.; Buttet, J.; Rabin, I.; Schulze, W.; Ertl, G. *Chem. Phys. Lett.* **1999**, *313*, 105.
(39) Wilcoxon, J. P.; Martin, J. E.; Parsapour, F.; Wiedenman, B.; Kelley, D. F. *J. Chem. Phys.* **1998**, *108*, 9137.
(40) He, P.; Shen, X.-H.; Gao, H.-C. *Acta Phys.-Chim. Sin.* **2004**, *20*, 1200.
(41) Ito, T.; Masumi, T. *J. Phys. Soc. Jpn.* **1997**, *66*, 2185.